Journal Name

COMMUNICATION

Oxidized Ti_3C_2 MXene Nanosheets for Dye-Sensitized Solar Cells

Chunxiang Dall'Agnese[a,†], Yohan Dall'Agnese[a,b,†], Babak Anasori[c], Wataru Sugimoto[a,b], Shogo Mori*[a,b]

Received 00th January 20xx,
Accepted 00th January 20xx

DOI: 10.1039/x0xx00000x

www.rsc.org/

Porous TiO_2 electrodes were prepared by oxidizing two-dimensional titanium carbide nanosheets (Ti_3C_2 MXene) and the electrodes were tested in dye-sensitized solar cells. The effects of oxidation temperature and duration time together with various thicknesses on the device performance were investigated. A power conversion efficiency of 2.66% was observed.

Recently, TiO_2 nanocrystals were synthesized by oxidation of two-dimensional (2D) titanium carbides, Ti_3C_2 and Ti_2C, by high temperature flash oxidation[1], annealing in CO_2 atmosphere at 850 °C[2] or 800 °C[3], chemical reaction[4], high-energy ball milling[5], calcination[6] and aging in air[7], respectively. These two carbides belong to a family of 2D materials called MXenes and are usually synthesized by selective etching of the A-element layer from their ternary carbide precursors, such as MAX phase[8-10]. Some MXenes, including Ti_3C_2, rheologically behave like clay and can be used to prepare additive-free flexible homogenous film[9]. MXenes have emerged as promising electrodes for energy storage devices such as batteries and electrochemical capacitors[10-12]. The partial or complete oxidation of MXenes into transition metal oxides have already been demonstrated and used to improve performance of lithium ion battery[1-4] and photocatalysis[5, 6].

TiO_2 has been used as mesoporous semiconductor electrodes for dye-sensitized solar cells (DSSCs)[13]. To prepare the electrode, typically paste containing 15-25 nm TiO_2 particles, organic dispersant and polymer binder is applied on a transparent conducting substrate (typically SnO_2:F, FTO, on a glass) and annealed at around 500 °C in air. Pore size and its distribution can be controlled by the amount of additives to the paste[14]. For electrolyte, I^-/I_3^- redox couple has been typically used for DSSCs. Since 2010, Co complexes have been commonly used as redox couple due to their more positive redox potential[15]. Since the size of the complexes is relatively large, the pore size of the electrodes needs to be enlarged to reduce the resistance against the diffusion of the Co complexes. However, if the pore size is enlarged, the mechanical strength of the film is decreased, making it difficult to fabricate thick TiO_2 films. Such films are needed to employ sensitizers whose absorption coefficients are low. For example, Ru complex dyes have wide absorption spectrum but low absorption coefficients. Thus, the dyes have not been utilized with Co complex redox couple because there is no method to fabricate thick and large pore TiO_2 electrodes. Therefore, it would be beneficial to explore alternative methods to fabricate porous TiO_2 electrodes rather than the method using a paste containing nanoparticles. Here, we propose the coating of MXenes nanosheets as precursor on FTO for the formation of porous TiO_2 film. To do so, we study the fabrication conditions to form porous TiO_2 films from the nanosheet and evaluate its performance in DSSCs. Then we discuss the applicability of the fabrication methods for DSSCs.

Fig. 1a shows X-ray diffraction (XRD) patterns of the as-deposited Ti_3C_2 film on FTO and the heat-treated films at different heating temperatures and time. After heating at 150 °C, the (002) and (004) peaks of Ti_3C_2 films were shifted to higher angles, corresponding to a 5.69 Å decrease of the *c*-lattice parameter, showing the desorption of a layer of water molecules that was trapped between Ti_3C_2 nanosheets during its synthesis and is coherent with previous work[16, 17]. After treatment at 250 °C for 30 min, the (002) peak almost disappeared, the (004) peak disappeared completely and peaks corresponding to rutile and anatase-type TiO_2 appeared. The formation of rutile at this temperature is not common, because rutile is usually synthetized at higher temperature[18, 19], except by hydrothermal method[20, 21]. It could be due to an effect of the substrate, or carbon doping, or oxygen vacancies but further

[a] Division of Chemistry and Materials, Faculty of Textile Science and Technology, Shinshu University, Ueda 386-8567, Japan.
[b] Center for Energy and Environmental Science, Shinshu University, 3-15-1 Tokida, Ueda, Nagano 386-8567, Japan
[c] A. J. Drexel Nanomaterials Institute, Materials Science and Engineering Department, Drexel University, 3141 Chestnut Street, Philadelphia, PA 19104, USA
† These authors contributed equally.
*E-mail: shogmori@shinshu-u.ac.jp
Electronic Supplementary Information (ESI) available. See DOI: 10.1039/x0xx00000x

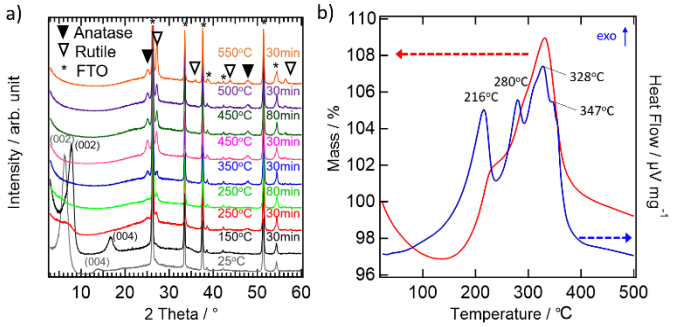

Fig. 1. XRD patterns of Ti_3C_2 coated on FTO electrodes for the pristine sample as well as the oxidized ones at different temperatures and duration times in air (a), and TG-DSC curves of Ti_3C_2 under air flow from room temperature to 500 °C (b).

work is needed to fully understand this phenomenon. When the oxidation time at 250 °C was extended to 80 min, the Ti_3C_2 oxidation reaction continued further and consequently the (002) peak disappeared in the corresponding XRD pattern. Concerning the samples oxidized at higher temperature, no peak position changed but the intensity of the peaks corresponding to TiO_2 increased with the temperature. Using the Scherrer equation[22] in the sample treated at 450 °C for 30 min, the crystal sizes of anatase and rutile TiO_2 are estimated to be 8 nm and 11 nm, respectively.

To further understand TiO_2 formation from the oxidation of Ti_3C_2 in air, the thermal stability of Ti_3C_2 was investigated by thermogravimetry and differential scanning calorimetry (TG-DSC), as shown in Fig. 1b. The initial mass loss from room temperature to 140 °C is attributed to desorption of water. The DSC curves present several exothermic peaks. As the mass increase from 140 °C to 334 °C, the peaks at 216 °C, 280 °C and 328 °C correspond to the oxidation of Ti_3C_2 into TiO_2 and carbon, supported by XRD spectra (Fig. 1a). Finally, above 334 °C, the mass loss corresponds to the oxidation of carbon to CO_2.

Fig. 2 shows cross-section field emission scanning electron microscope (FE-SEM) images of Ti_3C_2 films after heat treatment. As expected, after coating the Ti_3C_2 paste, the Ti_3C_2 nanosheets are horizontally aligned (Fig. S1a). Within the resolution of our SEM, the morphology did not change after heating at 150 °C for 30 min (Fig. 2a), nor after 30 min at 250 °C (Fig. 2b), despite of the fact that the peaks corresponding to TiO_2 particles were seen in the XRD pattern of the latter. After treatment at 250 °C for 80 min (Fig. 2c), the morphology became a mixture of particles and 2D layers. Based on XRD and TG-DSC results, and the previous work[1], it is probably a mixture of carbon and Ti_3C_2 nanosheets covered with TiO_2 nanoparticles. For electrodes prepared at higher temperature, i.e., 350 °C for 30 min (Fig. 2d), 450 °C for 30 min and 80 min (Fig. 2e and Fig. S1b), 500 °C for 30 min (Fig. S1c) and 550 °C for 30 min (Fig. S1d), only TiO_2 nanoparticles were observed. The morphologies of these films were similar to that of the films prepared from commercial TiO_2 paste (DSL-18NR-T) shown in Fig. 2f. However, the particles size of TiO_2 nanoparticles formed by oxidation of Ti_3C_2, ranging from 20 nm to 100 nm, were larger than that of DSL-18NR-T. The particles size of TiO_2 formed by Ti_3C_2 film treated at 450 °C for 30 min was further investigated by TEM (Fig. 2g) and compared

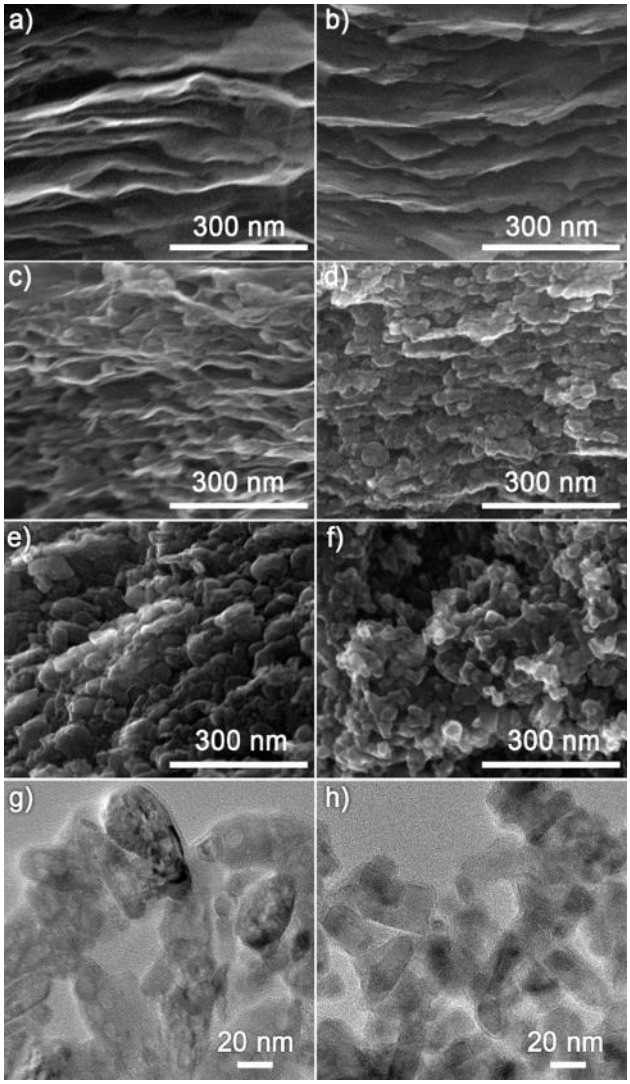

Fig. 2. FE-SEM images of coated Ti_3C_2 film treated at 150 °C for 30 min (a), at 250 °C for 30 min (b), at 250 °C for 80 min (c), at 350 °C for 30 min (d), at 450 °C for 30 min (e) and commercial DSL-18NR-T TiO_2 (f). TEM images of TiO_2 prepared from Ti_3C_2 at 450 °C for 30 min (g) and commercial DSL-18NR-T TiO_2 (h).

with that of DSL-18NR-T (Fig. 2h). The particles prepared from Ti_3C_2 were larger and more elongated, with average length of 60 ± 20 nm and width of 30± 10 nm. The size of DSL-18NR-T particles was in average 21 ± 4 nm.

The performances of DSSCs as a function of heating temperature and duration time were studied. Fig. 3 shows photocurrent density vs voltage (I-V) curves under one sun conditions and incident photon-to-current conversion efficiency (IPCE) spectra. Table 1 summarizes the corresponding photocurrent densities (J_{sc}), open-circuit voltages (V_{oc}), fill factors (FF), and power conversion efficiency (PCE). Both the J_{sc} and V_{oc} were increased and thus the increase of PCE when the oxidation temperature of Ti_3C_2 was increased from 150 °C to 450 °C. The efficiency of the device fabricated with Ti_3C_2 nanosheets heated at 150 °C was zero. This was due to the absence of semiconducting TiO_2 particle under this condition. The efficiency starts to increase for the sample oxidized at 250 °C and the cell performance was further improved by extending the heating time from 30 min to 80 min at relatively lower

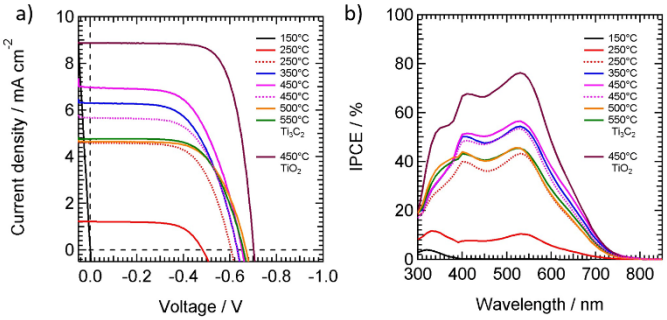

Fig. 3. I-V curves under one-sun conditions (a) and IPCE spectra (b) of DSSCs prepared from Ti_3C_2 nanosheets oxidized at various temperatures and duration time (solid line: 30 min; dashed line: 80 min). Commercial TiO_2 particles were used as reference.

Table 1. I-V characteristics of DSSCs as a function of Ti_3C_2 oxidation temperature and duration time. [a]

Oxidation temperature (°C)	Duration (min)	V_{oc} (V)	J_{sc} (mA/cm^2)	FF	PCE (%)
150	30	0	0.0968	0.930	0
250	30	0.481	1.22	0.663	0.389
250	80	0.607	4.60	0.632	1.76
350	30	0.634	6.30	0.583	2.33
450	30	0.652	6.97	0.585	2.66
450	80	0.629	5.67	0.612	2.18
500	30	0.670	4.65	0.634	1.97
550	30	0.656	4.76	0.639	2.00

[a] All film thicknesses were ca. 6 µm.

temperature (250 °C). This is consistent with Ti_3C_2 oxidation, which leads to more TiO_2 particles formation. However, oxidation at 450 °C for 80 min and higher temperatures (500 °C and 550 °C) decrease device performance from 2.66% to about 2%. This could be due to smaller surface area of the electrodes caused by growth of the particles.

Based on Table 1, our best electrode forms by oxidizing Ti_3C_2 at 450 °C for 30 min. The device performance was further studied with various TiO_2 film thicknesses under the best oxidizing condition. The I-V characteristics are described in Table 2. The cell performance increased with film thickness up to about 6 µm, and then, decreased. For comparison, DSSCs were fabricated with commercially available TiO_2 (DSL-18NR-T) particles (Table 2).

Table 2. *I-V* characteristics of DSSCs using various TiO_2 films thicknesses by oxidizing Ti_3C_2 films with desired thicknesses at 450 °C for 30 min, and using TiO_2 film obtained by annealing commercial DSL-18NR-T paste at 450 °C for 30 min.

Films	Film thickness (µm)	V_{oc} (V)	J_{sc} (mA/cm^2)	FF	PCE (%)
Oxidized Ti_3C_2	3.6	0.670	4.57	0.622	1.90
	3.9	0.674	5.48	0.608	2.25
	6.4	0.652	6.97	0.585	2.66
	10.2	0.594	5.70	0.610	2.06
	12.2	0.607	5.16	0.626	1.96
TiO_2 (DSL-18NR-T)	5.7	0.702	8.88	0.725	4.52

To understand the lower performance of the DSSCs using TiO_2 electrodes prepared by oxidizing Ti_3C_2 nanosheets, charge transport and recombination kinetics were investigated, as shown in Fig. 4. The electron diffusion coefficient in the electrodes prepared from DSL-18NR-T TiO_2 was about 10-fold higher than that in the film prepared from Ti_3C_2, while the electron lifetime in DSL-18NR-T films was more than two orders of magnitude shorter than that in the counterpart. To obtain high charge collection efficiency, electron diffusion length, which is the square root of the product of diffusion coefficient and lifetime, should be larger than the thickness of the TiO_2 film. The results of the diffusion coefficient and lifetime measurements suggest that the electron diffusion length in the films prepared from Ti_3C_2 is not the reason of the low solar cell performance. Table 2 shows the decrease of J_{sc} values with thick electrodes. During cell preparation, these thick films were detached easily compared to thinner films. These results imply that the decreased J_{sc} with thick electrodes might be due to high electrical resistance in the oxidized Ti_3C_2 (i.e., TiO_2) films and/or at FTO/TiO_2 interface. The V_{oc} of the DSSCs prepared from Ti_3C_2

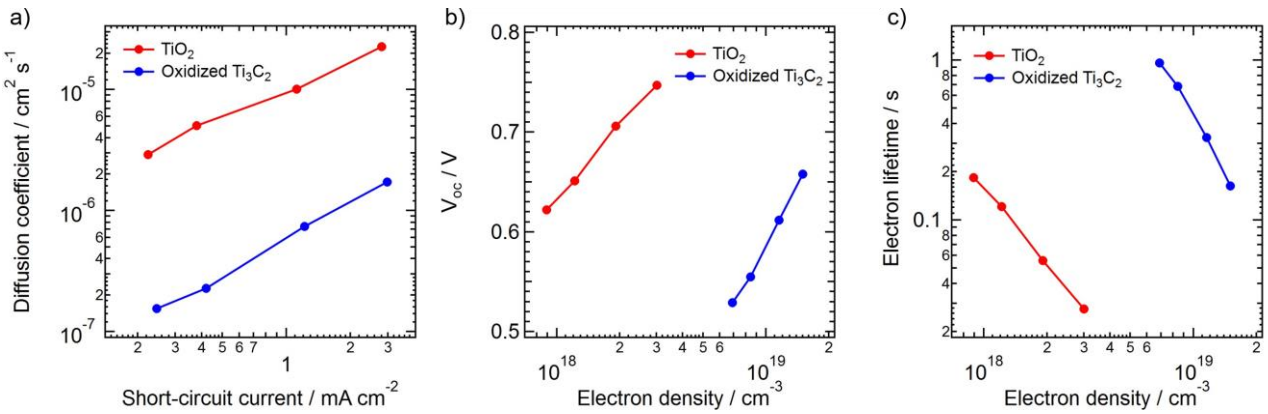

Fig. 4. Relationship between electron diffusion coefficient and short-circuit current (a), open-circuit voltage and electron density (b), and electron lifetime and electron density (c) in DSSCs prepared from oxidization of Ti_3C_2 and commercial TiO_2.

was about 300 mV lower than that of DSSCs prepared from DSL-18NR-T at matched electron density. Such large difference is hardly expected due to the shift of the TiO_2 conduction band edge potential. On the other hand, the plots of diffusion coefficient, lifetime and V_{oc} in Fig. 4 can be interpreted consistently if the TiO_2 films prepared from Ti_3C_2 have higher density of charge traps. Note that for this case, the charge traps on TiO_2 surface do not act as recombination center but slow down the electron transport to meet acceptor species at the TiO_2 surface, resulting longer electron lifetime. Since the traps slow both the electron transport and recombination, the trap density does not influence the electron diffusion length. However, the traps often decrease the Fermi level of TiO_2 even though the electron density in the TiO_2 is increased due to slower charge recombination. Therefore, to improve the efficiency of the DSSCs, the trap density of the TiO_2 films prepared from Ti_3C_2 should be decreased. The origin of traps has not been elucidated completely. One origin could be simple crystal defects but it seems the traps are formed more inherently due to nano-sized structure. Thus, probably one cannot remove all the traps. A hint could be found from a general trend, that is, particles showing clear crystal facets seem to have less charge trap density for DSSCs. Along the direction, to obtain flat surface TiO_2 particle/film, oxidation condition/method for Ti_3C_2 should be developed.

The amount of adsorbed dyes on the electrodes prepared from oxidized Ti_3C_2 at 450 °C for 30 min and DSL-18NR-T TiO_2 paste annealed at 450 °C for 30 min was evaluated by measuring the absorbance of dissolved dyes in NaOH (10 mM) aqueous solution. The amounts of adsorbed-dye on the films from this oxidized Ti_3C_2 and DSL-18NR-T TiO_2 paste were about $1.2x10^{-4}$ and $1.7x10^{-4}$ mol/cm^{-3}, respectively. This is consistent with the larger size of the particles prepared from Ti_3C_2 oxidation than that of DSL-18NR-T TiO_2 as shown in Fig. 2. The lower values of J_{sc} for Ti_3C_2 based DSSCs were partially due to its lower dye loading.

Another problem of the present DSSCs prepared from the nanosheets is its low fill factor. Since the porous structure was formed from nanosheets laying on FTO substrate, one possible reason of low FF could be due to insufficient pore channels along the vertical axis, increasing the diffusion resistance for redox couples to the Pt counter electrode. On the other hand, from different point of view, this would lead to an idea that if the nanosheets can be vertically placed on the substrate and oxidized, larger pore along the vertical axis may be formed. Such structure is desired for DSSCs using large sized molecules for redox couples or using solid-state hole conductor[23, 24]. The pore size and TiO_2 particle size may be controlled by the addition of polymer into the paste[14, 25-27]. Thus, the method we demonstrated here would open possibility to control the porous structure more precisely than the conventional methods using TiO_2 nanoparticles.

In summary, porous TiO_2 electrodes were formed by oxidizing Ti_3C_2 MXene nanosheets. Paste was prepared only with water and Ti_3C_2 nanosheets, and the sheets were oxidized into porous film consisting of rutile and anatase TiO_2 nanoparticles by simple heating in air. DSSCs were fabricated from the electrodes prepared with different heating temperatures and different thicknesses. The highest efficiency was obtained from the 6.4-µm-thick film prepared at 450 °C but the efficiency was lower than DSSCs prepared from commercially available TiO_2 nanoparticles. The lower performance was explained by a lower surface area, higher charge traps of the films, and undesired pore structure. On the other hand, no inherent problems were found, suggesting the possibility of improvement of the proposed method to produce high-performance oxide films for solar cell applications.

This work was partially supported by JSPS KAKENHI Grant Number JP26288089. The authors greatly thank Prof. Yury Gogotsi for his helpful comments on the manuscript.

Conflicts of interest

The authors declare no competing financial interests.

Notes and references

1. M. Naguib, O. Mashtalir, M. R. Lukatskaya, B. Dyatkin, C. Zhang, V. Presser, Y. Gogotsi and M. W. Barsoum, *Chemical Communications*, 2014, **50**, 7420-7423.
2. C. Zhang, S. J. Kim, M. Ghidiu, M.-Q. Zhao, M. W. Barsoum, V. Nicolosi and Y. Gogotsi, *Advanced Functional Materials*, 2016, **26**, 4143-4151.
3. M.-Q. Zhao, X. Xie, C. E. Ren, T. Makaryan, B. Anasori, G. Wang and Y. Gogotsi, *Advanced Materials*, 2017, **29**, 1702410.
4. B. Ahmed, D. H. Anjum, M. N. Hedhili, Y. Gogotsi and H. N. Alshareef, *Nanoscale*, 2016, **8**, 7580-7587.
5. J. Li, S. Wang, Y. Du and W. Liao, *Ceramics International*, 2018, **44**, 7042-7046.
6. J. Low, L. Zhang, T. Tong, B. Shen and J. Yu, *Journal of Catalysis*, 2018, **361**, 255-266.
7. J. Halim, K. M. Cook, M. Naguib, P. Eklund, Y. Gogotsi, J. Rosen and M. W. Barsoum, *Applied Surface Science*, 2016, **362**, 406-417.
8. M. Naguib, O. Mashtalir, J. Carle, V. Presser, J. Lu, L. Hultman, Y. Gogotsi and M. W. Barsoum, *ACS Nano*, 2012, **6**, 1322-1331.
9. M. Ghidiu, M. R. Lukatskaya, M.-Q. Zhao, Y. Gogotsi and M. W. Barsoum, *Nature*, 2014, **516**, 78-81.
10. B. Anasori, M. R. Lukatskaya and Y. Gogotsi, *Nature Reviews Materials*, 2017, **2**, 16098.
11. M. Naguib, J. Come, B. Dyatkin, V. Presser, P.-L. Taberna, P. Simon, M. W. Barsoum and Y. Gogotsi, *Electrochemistry Communications*, 2012, **16**, 61-64.
12. M. R. Lukatskaya, O. Mashtalir, C. E. Ren, Y. Dall'Agnese, P. Rozier, P. L. Taberna, M. Naguib, P. Simon, M. W. Barsoum and Y. Gogotsi, *Science*, 2013, **341**, 1502-1505.
13. B. O'Regan and M. Grätzel, *Nature*, 1991, **353**, 737-740.
14. Y. Saito, S. Kambe, T. Kitamura, Y. Wada and S. Yanagida, *Solar Energy Materials and Solar Cells*, 2004, **83**, 1-13.
15. S. M. Feldt, E. A. Gibson, E. Gabrielsson, L. Sun, G. Boschloo and A. Hagfeldt, *Journal of the American Chemical Society*, 2010, **132**, 16714-16724.
16. M. Ghidiu, J. Halim, S. Kota, D. Bish, Y. Gogotsi and M. W. Barsoum, *Chemistry of Materials*, 2016, **28**, 3507-3514.
17. K. D. Fredrickson, B. Anasori, Z. W. Seh, Y. Gogotsi and A. Vojvodic, *The Journal of Physical Chemistry C*, 2016, **120**, 28432-28440.

18. D. A. H. Hanaor and C. C. Sorrell, *Journal of Materials Science*, 2011, **46**, 855-874.
19. C.-C. Wang and J. Y. Ying, *Chemistry of Materials*, 1999, **11**, 3113-3120.
20. H. Y. Zhu, Y. Lan, X. P. Gao, S. P. Ringer, Z. F. Zheng, D. Y. Song and J. C. Zhao, *Journal of the American Chemical Society*, 2005, **127**, 6730-6736.
21. B. Liu and E. S. Aydil, *Journal of the American Chemical Society*, 2009, **131**, 3985-3990.
22. P. Scherrer, *Bestimmung der Größe und der inneren Struktur von Kolloidteilchen mittels Röntgenstrahlen, Nachrichten von der Gesellschaft der Wissenschaften zu Göttingen*, 1918, **2**, 98-100.
23. L. Gonzalez-Garcia, I. Gonzalez-Valls, M. Lira-Cantu, A. Barranco and A. R. Gonzalez-Elipe, *Energy & Environmental Science*, 2011, **4**, 3426-3435.
24. D. Kim, A. Ghicov, S. P. Albu and P. Schmuki, *Journal of the American Chemical Society*, 2008, **130**, 16454-16455.
25. S. H. Ahn, D. J. Kim, D. K. Roh, W. S. Chi and J. H. Kim, *ChemPhysChem*, 2014, **15**, 1841-1848.
26. J. K. Kim, C. S. Lee, S.-Y. Lee, H. H. Cho and J. H. Kim, *Journal of Power Sources*, 2016, **336**, 286-297.
27. M. A. Abdolahi Sadatlu and N. Mozaffari, *Solar Energy*, 2016, **133**, 24-34.